Journal of Fluids and Structures (2000) **14,** 197–219
doi: 10.1006/jfls. 1999.0259, available online at http://www.idealibrary.com on IDEAL®

FLOW PERIODICITY AND ACOUSTIC RESONANCE IN PARALLEL TRIANGLE TUBE BUNDLES

S. ZIADA

Department of Mechanical Engineering, McMaster University
Hamilton, Ontario, Canada

AND

A. OENGÖREN

Fluid Dynamics Department, Sulzer Innotec Limited
Winterthur, Switzerland

(Received 7 January 1998 and in revised form 27 July 1999)

Parallel triangle tube arrays with pitch ratios in the range of 1·2–4·2 have been tested at Reynolds numbers up to 9×10^4 to investigate the vorticity shedding and acoustic resonance mechanisms. Three different components of flow periodicities have been observed. The flow periodicity with the highest Strouhal number (S_3) is the weakest component. It is caused by a shear-layer instability in small pitch ratio arrays and at low Reynolds numbers. The S_2 component is associated with small-scale vortex shedding at the first row. The third component has the lowest Strouhal number (S_1) and is the strongest. It is generated by large-scale, alternating vortex shedding at deeper rows, and it becomes dominant at all rows at high Reynolds numbers. For tube arrays with pitch ratios less than 3·4, the onset of acoustic resonances could not be related to the natural flow periodicities mentioned above. This behaviour is in contrast with that of normal triangle arrays, but similar to the acoustic behaviour of in-line arrays. Strouhal number charts for the natural flow periodicities and for the onset of acoustic resonances have been developed.

1. INTRODUCTION

FLOW-INDUCED ACOUSTIC and mechanical vibrations of heat exchanger tube bundles have been the topic of numerous studies in the literature since such vibrations often cause costly damage or unacceptably noisy working conditions in applications such as the process and power industries. The main objective of many of these studies has been to collect data to help develop guidelines which can be used to predict the occurrence of flow-induced vibrations at the design stage and thereby implement counter-measures to avoid vibration and noise problems.

The tube arrays used in practical applications of heat exchangers have diverse geometries, necessitated by optimization of the equipment efficiency in each particular application. This diversity leads to different flow phenomena that can excite acoustic resonances or mechanical vibrations. Early attempts to describe these flow phenomena resulted in some controversies regarding the nature of the flow excitation (Païdoussis 1982; Weaver 1993). However, research efforts in the last two decades have shown beyond a doubt that the nature of the excitation mechanisms differs as the tube array configuration is changed, for instance, from an in-line to a staggered array (Ziada & Oengören 1992; Weaver 1993). There is also evidence in the results of some recent studies (Weaver *et al.* 1993; Price *et al.* 1995;

0889–9746/00/020197 + 23 $35.00/0

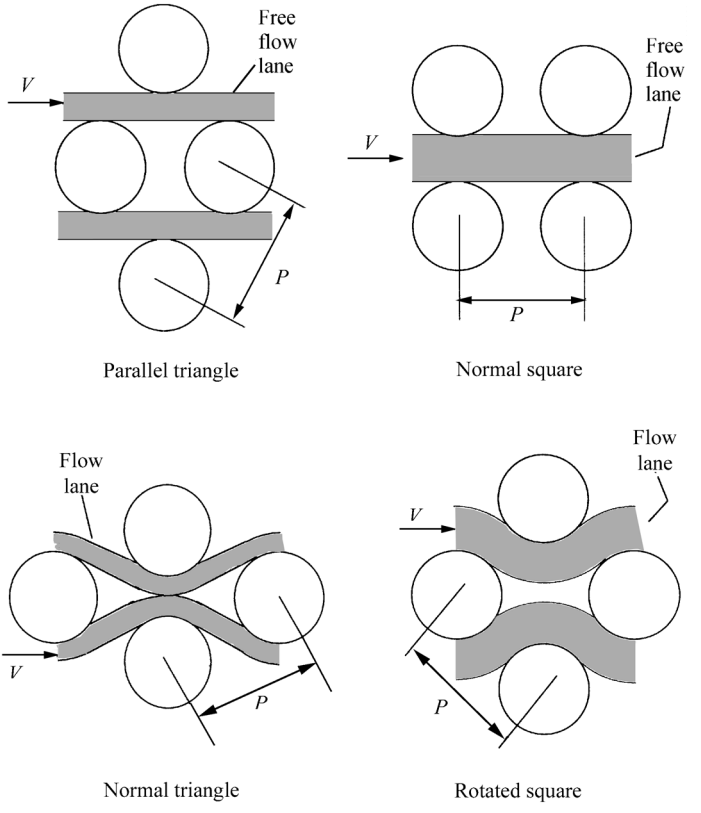

Figure 1. Standard layout patterns of tube arrays and corresponding patterns of flow "lanes" for a selected pitch ratio ($P/d = 1{\cdot}4$).

Oengören & Ziada 1998) that the flow and resonance characteristics of normal triangle (NTR), parallel triangle (PTR) and rotated square (RSQ) arrays, which belong to the category of staggered arrays, have some fundamental differences.

These differences can be attributed to variations in the layout pattern of the tubes. Parallel triangle arrays have staggered tubes similar to those in NTR and RSQ arrays. However, in contrast to the latter, they allow the flow to proceed relatively freely along the lanes between adjacent tube columns. This feature is similar to that of in-line arrays. A sketch illustrating the geometric differences in arrays having the same pitch ratio is shown in Figure 1. In the literature, the flow structures in NTR and RSQ arrays are observed to be dominated by a wake instability (Weaver *et al.* 1993; Polak & Weaver 1995; Oengören & Ziada 1998), whereas those in in-line arrays are controlled by a jet instability (Ziada & Oengören 1992). As a result of being under the effect of combined geometrical constraints of these two categories, i.e., in-line and staggered, the flow mechanisms in parallel triangle arrays may exhibit more complex characteristics.

This study focuses on the vorticity shedding mechanism in parallel triangle tube arrays. The effects of Reynolds number as well as row depth on this mechanism are investigated for a wide range of pitch ratio. The acoustic responses of the tested arrays are also studied, and attempts are made to identify the excitation sources. Of the 8 pitch ratios investigated, three are discussed in detail to elucidate differences in the flow features of small, intermediate and large spacing arrays. The results from other pitch ratios are referred to wherever necessary.

Finally, Strouhal number charts for the natural vorticity excitation and for the onset of acoustic resonances are presented.

2. EXPERIMENTAL FACILITY

2.1. Air Tests

The air tests were conducted in an open circuit wind tunnel. Detailed descriptions of its geometric and flow characteristics are given by Oengören and Ziada (1992b). Here, only the information essential to understand the tests of this study will be repeated.

The tests were conducted in a rectangular test section, 200 mm in width and 520 mm in height. Acrylic rods simulating the tubes were rigidly mounted on the test-section side walls, which were made of 10 mm thick steel plates. Half-tubes were mounted on the top and bottom walls to minimize mean flow distortion. A detailed overview of the geometrical parameters of the tested bundles is given in Table 1. Eight different parallel triangle arrays were tested. By changing the pitch and diameter of the tubes, the tube pitch ratio was varied in the range of $1{\cdot}21 < X_p{}^{\dagger} < 4{\cdot}17$. An overall view of the tube array configuration and the measurement locations is shown in Figure 2(a).

The sound pressure level (SPL) was measured by $\frac{1}{4}''$ condenser microphones located on the top wall of the test section at mid-depth of the bundle. The local pressure fluctuations on the tubes were detected by a microphone connected to a 1 mm diameter pressure tap drilled on the top surface of the tubes, i.e., at 90° to the flow direction. The use of this technique in assessing the unsteady flow characteristics in tube bundles has been verified in a previous study by means of the signal of a hot wire located near the pressure tap. For further details, see Oengören & Ziada (1998).

2.2. Water Tests

Three of the arrays tested in air, $X_p = 1{\cdot}44$, $2{\cdot}08$ and $3{\cdot}41$, were also tested in water, see Table 1. The water tests were conducted in a closed-loop water channel facility. The test-section had a cross-section of 300×400 mm. The diameter of the tubes were so chosen that at least six full tubes (five full and two half-tubes) could be fitted in the test-section in each case. The tubes were vertically mounted in the test-section. A sketch showing the tube array configuration used in the water tests is given in Figure 2(b). It was not possible to keep all geometric parameters the same in both air and water tests, e.g. span ratio and number of tube rows/columns. However, these geometrical differences did not affect the results since it was possible to generate similar mechanisms in both air and water tests.

In the water tests, it was possible to generate self-excited free-surface waves, which simulate the acoustic resonance phenomena observed in the air tests. This simulation technique has been discussed in detail by Ziada & Oengören (1992, 1993). The mean and fluctuating flow components were measured by means of hot-film anemometry. Flow visualization was carried out with the aid of a split-screen video system, so that the flow pattern observed between the tubes and the hot-film signal generated by this pattern could be displayed simultaneously on the screen. The signals detected by either pressure or hot-film probes were processed by a multichannel real-time analyser.

[†]Refer to Appendix for definition of this and other quantities.

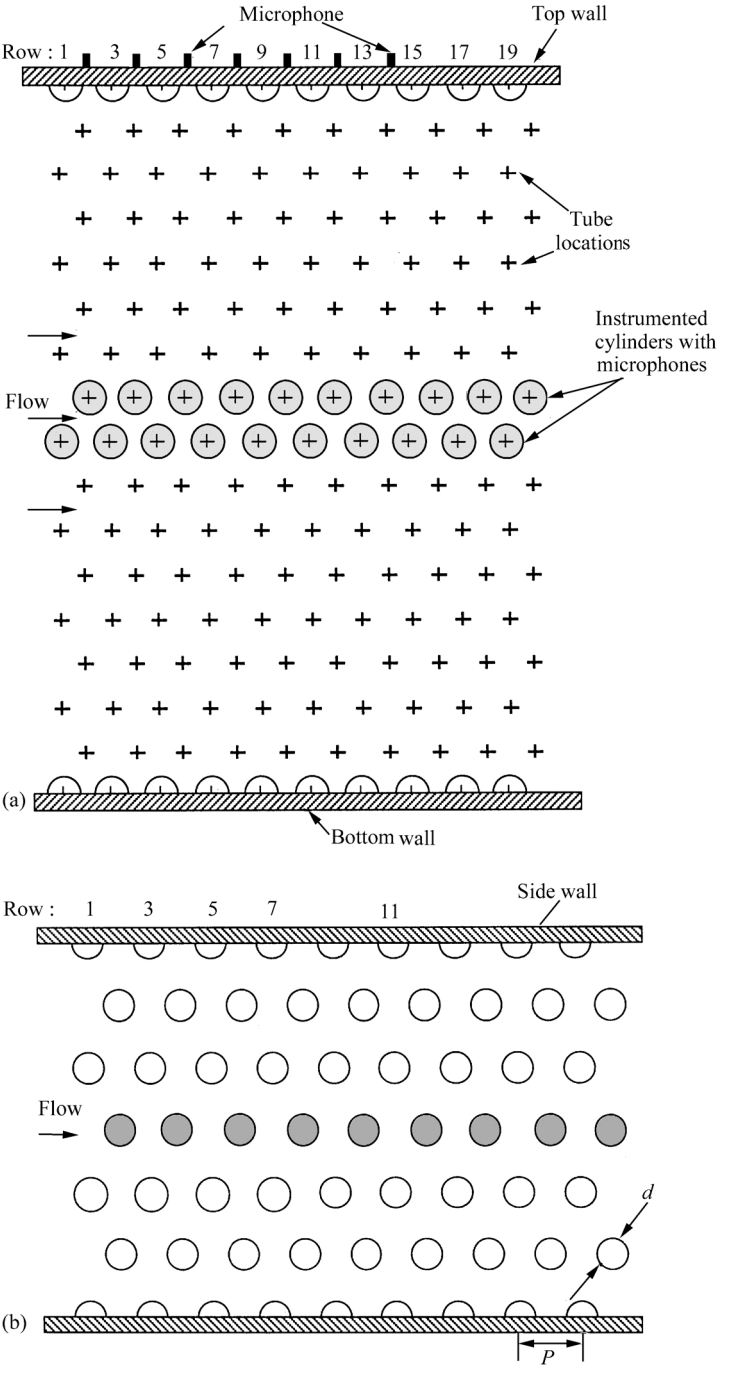

Figure 2. Overviews of the tube array test sections used in (a) air tests and (b) water tests.

3. FLOW PERIODICITIES IN PARALLEL TRIANGLE ARRAYS

In the following, the unsteady flow features in a selected array of each pitch-ratio category (i.e., small, intermediate and large pitch ratios) will be discussed in detail. The conclusions

TABLE 1

Geometrical parameters of tested arrays

Tube pitch ratio, $X_p = P/d$	Tube diameter d (mm)	Tube span ratio	Number of tube rows	Number of tube columns
Air Tests				
1·21	31	6·45	23	$15 + 2 \times (\frac{1}{2})$
1·44	26	7·69	23	$15 + 2 \times (\frac{1}{2})$)
1·71	22	9·09	23	$15 + 2 \times (\frac{1}{2})$
1·88	20	10·0	23	$15 + 2 \times (\frac{1}{2})$
2·08	18	11·1	23	$15 + 2 \times (\frac{1}{2})$
2·42	31	6·45	11	$7 + 2 \times (\frac{1}{2})$
3·41	22	9·09	11	$7 + 2 \times (\frac{1}{2})$
4·17	18	11·1	11	$7 + 2 \times (\frac{1}{2})$
Water Tests				
1·44	25	16·0	17	$7 + 2 \times (\frac{1}{2})$
2·08	25	16·0	17	$7 + 2 \times (\frac{1}{2})$
3·41	16	25·0	17	$5 + 2 \times (\frac{1}{2})$

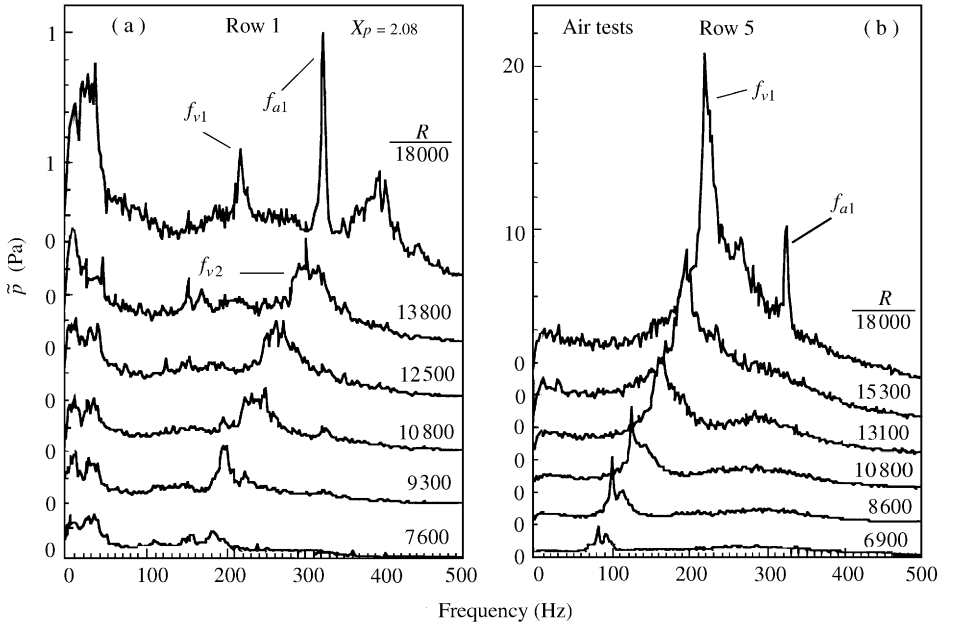

Figure 3. Pressure spectra measured on the tubes of (a) row 1 and (b) row 5 in the intermediate pitch-ratio array for a Reynolds number range of $6900 < R < 18\,000$. $X_p = 2{\cdot}08$, air tests.

drawn from the results of these arrays will be supported by additional data obtained from other arrays of the same pitch-ratio category.

3.1. INTERMEDIATE PITCH RATIO ARRAY ($X_P = 2{\cdot}08$)

Two series of pressure spectra measured on rows 1 and 5 of the array with $X_P = 2{\cdot}08$ are shown in Figure 3 for a Reynolds number range of $6900 < R < 18\,000$. These spectra show

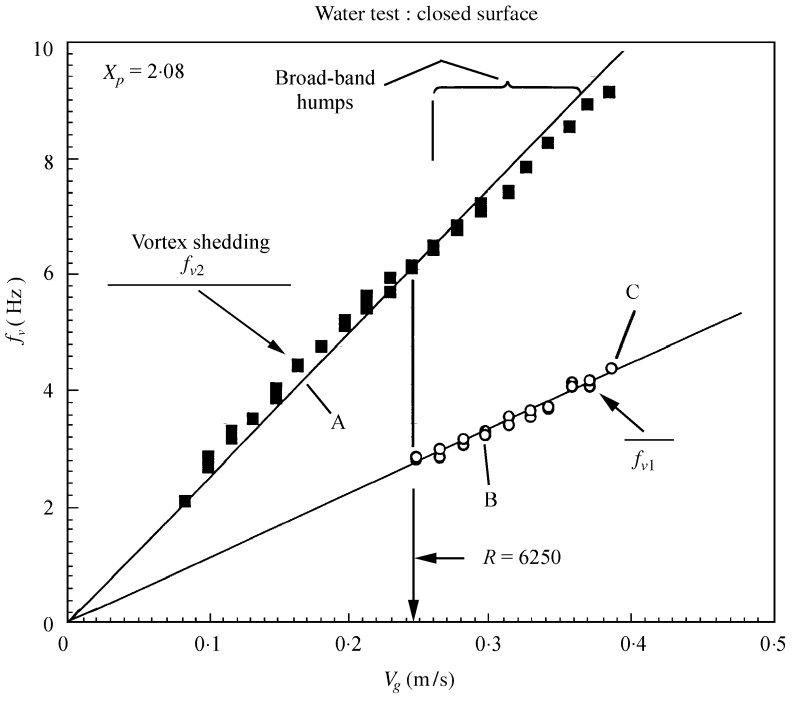

Figure 4. Frequencies of the flow periodicities observed behind row 1 in the intermediate pitch-ratio array ($X_p = 2{\cdot}08$) as a function of gap velocity. Water tests.

that the pressure fluctuations on the tubes occur at multiple frequencies. Although a single-frequency component is observed in the spectra of each row, these components have different frequencies and correspond to different Strouhal numbers. This suggests that the unsteady flow structures occurring at these rows are different. The component f_{v1} is detected at row 5 and has a Strouhal number of $S_1 = 0{\cdot}28$, whereas f_{v2} is measured at row 1 and corresponds to $S_2 = 0{\cdot}48$. Both of these components exist simultaneously in the array, regardless of the Reynolds number, indicating that a transition takes place from the periodic structures S_2 to S_1 as the flow proceeds into the array. The component f_{v1} is enhanced at higher Reynolds numbers and its amplitude becomes an order of magnitude larger than that of f_{v2} at $R = 18\,000$. Above this Reynolds number, this component becomes detectable even at row 1, as displayed in Figure 3(a). It is noteworthy here that at $R = 18\,000$, an enhancement of the first acoustic mode (f_{a1}) is observed in both spectra, which indicates the onset of resonance although the component S_1 is still significantly lower than the resonance frequency, and the component S_2 has already passed this frequency without causing any resonance effect.

The dependence of the flow periodicity on Reynolds number is further delineated in Figure 4, where the frequency of vortex shedding behind row 1 is plotted against the gap velocity. Figure 5 shows typical spectra taken at the test conditions symbolized by letters A, B and C in Figure 4. Data shown in Figures 4 and 5 are obtained from the water tests, where acoustic excitation does not affect the vortex-shedding phenomenon. At low velocities ($R < 6250$), only the f_{v2} component appears behind row 1. As the flow velocity is increased, the f_{v1} component gains in strength at the rear rows and becomes apparent in the spectra measured behind the first row. Both components exist in the spectra when $R > 6250$. This is in agreement with the observations of air tests. As indicated in Figure 5, the f_{v2} component

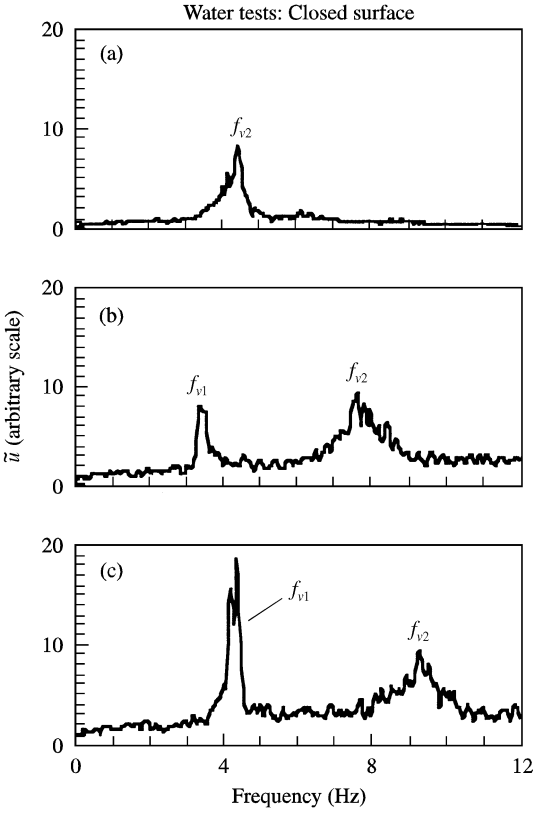

Figure 5. Hot-film spectra measured at three different flow velocities corresponding to cases A, B and C in Figure 4.

seems to become broad-banded at high velocities ($V_g > 0{\cdot}3$ m/s). However, this is believed to be associated with the increase in the turbulence level resulting from the surface ripples that form at the upstream side of the test section. In fact, comparison of the three spectra given in Figure 5 indicates that the maximum amplitude of the humps corresponding to this frequency component remains at about the same level in the tested Reynolds number range.

The two photographs given in Figure 6 display the flow patterns behind the first row obtained from the water tests of the same array at a relatively low Reynolds number ($R = 1870$). The Strouhal number corresponding to the well-defined vortices observed in these photographs is determined to be 0·46 from the video counting. This Strouhal number corresponds to the component f_{v2}, which is sensed by the hot film in water, and it corresponds to S_2, which is measured at the first row in the air tests. Figure 6 also shows that vortex shedding behind the first row forms in two different patterns, a symmetric and an antisymmetric pattern (bottom and top photographs, respectively). The change from one pattern to the other is observed to occur randomly and the vortices of both patterns are shed with the same frequency.

In Figure 7, a set of flow visualization photographs exhibiting the main features of flow activities at a relatively high Reynolds number ($R = 12\,300$) is given. The photographs are phase related, and so they represent the global structure developing in this array at a given instant of time. Minimal flow unsteadiness is observed behind the first two rows. Coherent flow structures appear first behind the fifth row where well-defined vortices are shed from

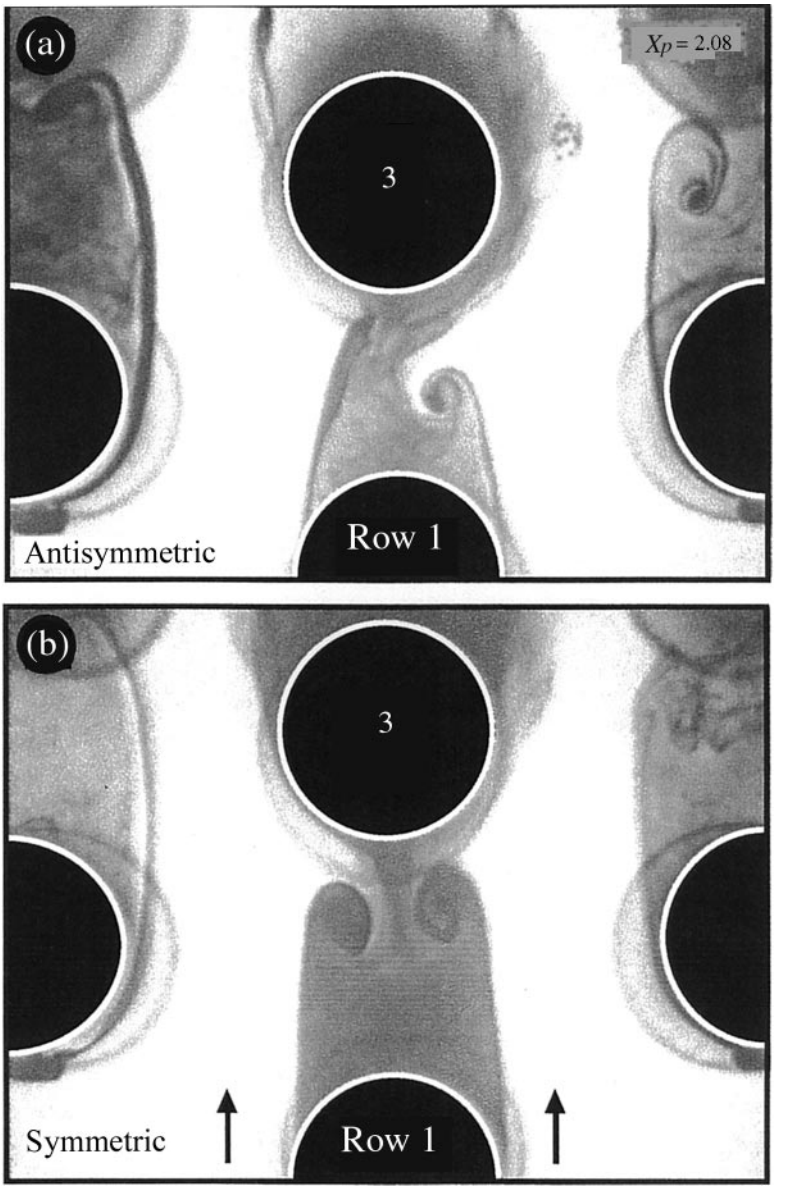

Figure 6. Flow visualization photographs showing the flow patterns associated with the flow periodicity S_2. Intermediate pitch-ratio array, $X_p = 2{\cdot}08$, $R = 1870$.

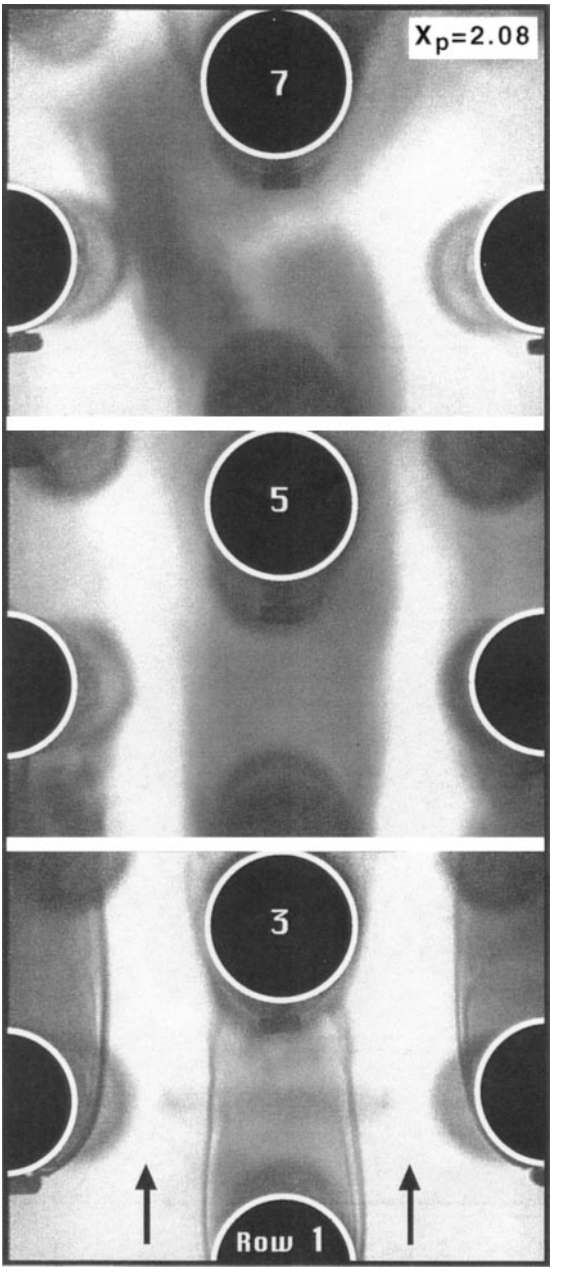

Figure 7. Streamwise development of the flow structure associated with the flow periodicity S_1. Intermediate pitch-ratio array, $X_p = 2{\cdot}08$, $R = 12\,300$.

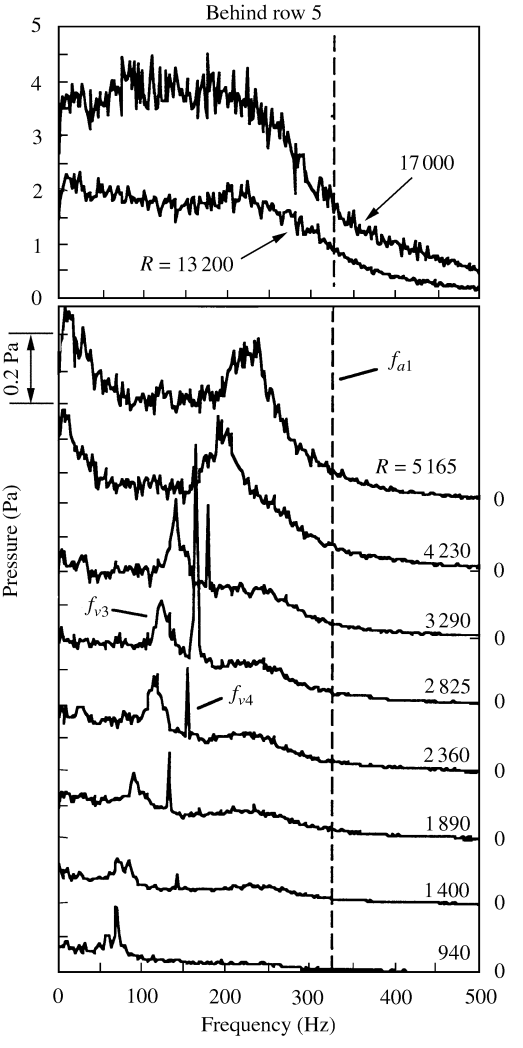

Figure 8. Spectra of pressure fluctuations on row 5 of the small pitch-ratio array for several Reynolds numbers. Air tests, $X_p = 1{\cdot}44$.

the tubes of this row. The shedding vortices are as large as the tube diameter and have a Strouhal number of $\sim 0{\cdot}24$ from the video counting. This value agrees with the component f_{v1} of the air tests suggesting that they represent the same flow periodicity.

3.2. Small Pitch-Ratio Array ($X_P = 1{\cdot}44$)

The tube array with $X_p = 1{\cdot}44$ is discussed here in detail as a representative example of the arrays with small pitch ratios. In Figure 8, a series of pressure spectra measured at the fifth row in this array is shown for a Reynolds number range of $940 < R < 17\,000$. As seen in this figure, similar to the intermediate pitch-ratio array, the flow has a multiple frequency nature for a relatively large Reynolds number range. However, the peaks appearing in Figure 8 are found to be associated with different flow structures and, therefore, they are designated as f_{v3} and f_{v4}, instead of f_{v1} and f_{v2} as in the intermediate pitch-ratio array. This designation is

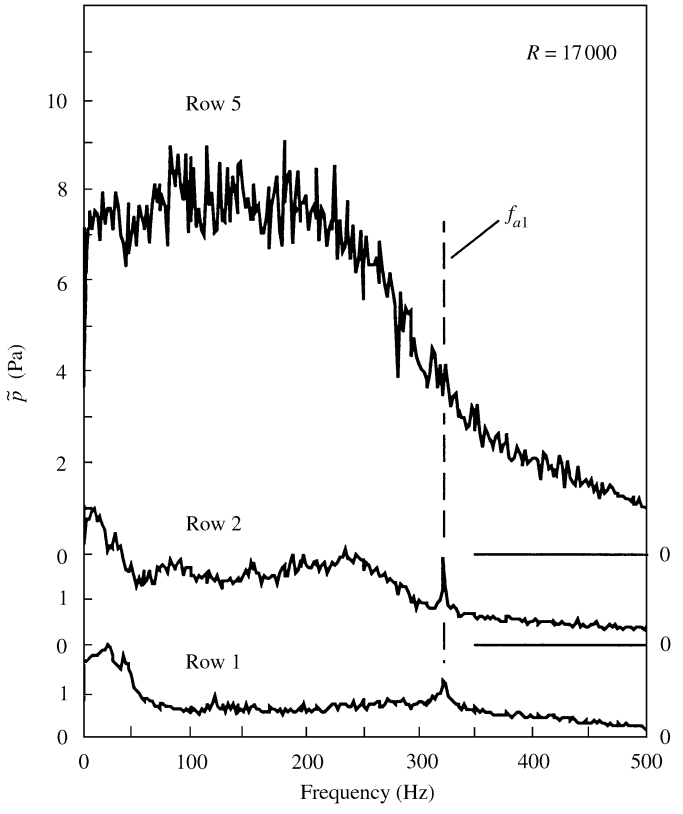

Figure 9. Pressure spectra measured on rows 1, 2 and 5 of the small pitch-ratio array at a Reynolds number of $R = 17\,000$. Air tests, $X_p = 1{\cdot}44$.

made because the Strouhal numbers corresponding to the former peaks are much higher than those of the latter.

In Figure 8, it is shown that the flow periodicity appears first as a single-frequency event, f_{v3}, at very low Reynolds numbers, $R = 1400$. As the Reynolds number is increased over 1400, the second component, f_{v4}, which is much sharper and stronger than f_{v3}, appears in the pressure spectra. This peak persists and even gains in strength within the range $1890 < R < 3290$, but disappears abruptly when R is increased beyond this range. These characteristics suggest that the component f_{v4} is generated by a local discrete-flow phenomenon which could not be identified in this study.

On the other hand, the f_{v3} component persists over a larger range of Reynolds number, $0 < R < 5165$. However, it generally transforms into a broad-banded event and eventually ceases to exist when R is increased over 5165. Thereafter, the pressure spectra measured at row 5 for $R > 5165$ display the characteristics of a turbulent flow as observed clearly in the top two spectra of Figure 8. The onset of a totally turbulent flow in the high Reynolds number range also appears in the spectra measured at the first two rows of this array. This feature is illustrated in Figure 9, where the pressure spectra on the first two rows are compared with that on row 5 for a Reynolds number of 17 000. None of these spectra contains discrete components, indicating that periodic events disappear through the whole bundle. The peak appearing in the spectra of rows 1 and 2 around a frequency of 324 Hz belongs to the first acoustic cross mode of the test section, f_{a1}. This acoustic peak could be

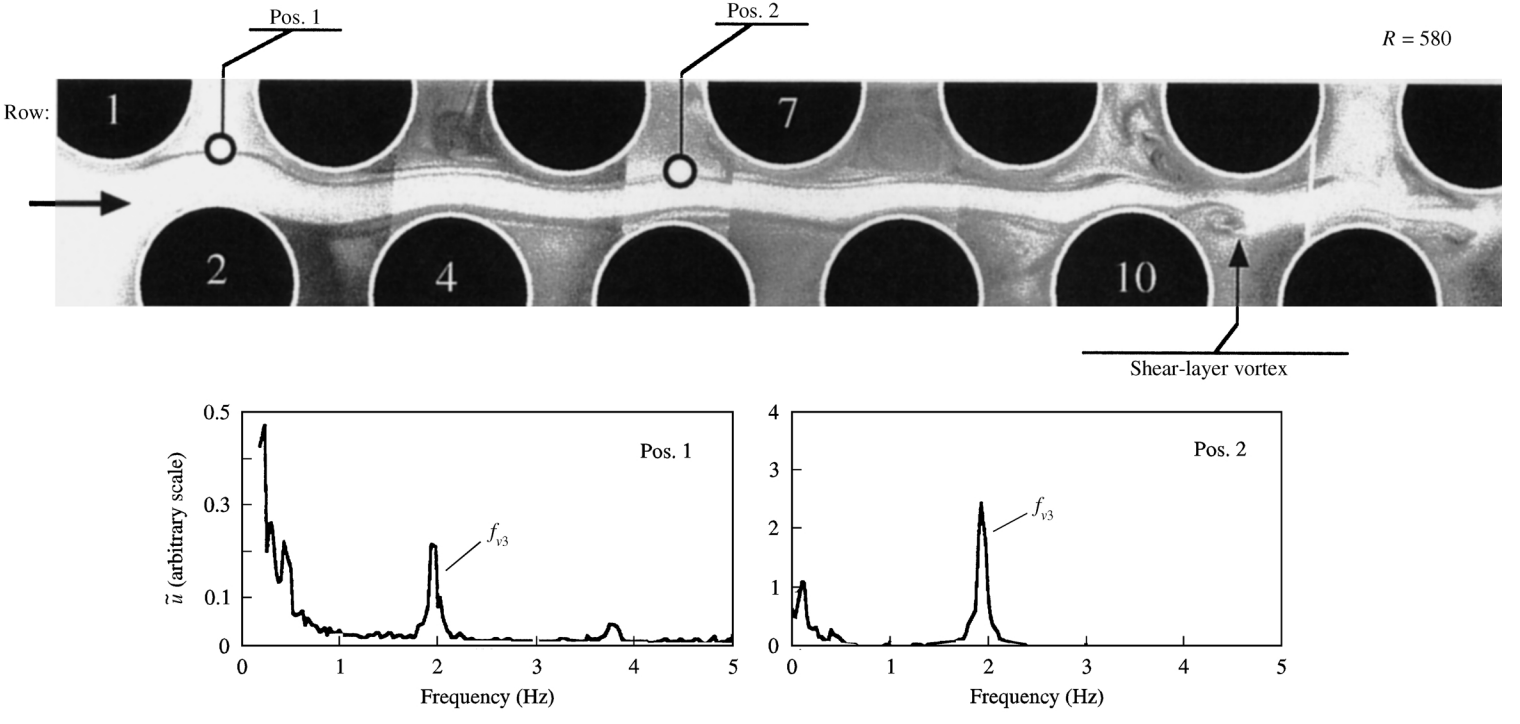

Figure 10. Flow patterns observed in a flow lane of the array with $X_p = 1{\cdot}44$ at a Reynolds number of $R = 580$ and the corresponding hot-film spectra measured behind rows 1 and 5 in water.

detected at the front rows since the turbulence level is still low at this location. However, it does not represent a resonance and it could not be detected in the spectra of the fifth row since its amplitude is small compared to the turbulence level at this location.

The flow periodicities occurring in the array with $X_p = 1{\cdot}44$ are further investigated in the water channel with a tube bundle model having the same array geometry as the one tested in air. Figure 10 shows visualization of the flow pattern in a flow lane from the first to the 11th row at a Reynolds number of 580. The flow proceeds in the free lane between the two tube columns displayed in this figure. The shear layers developing on both sides of the flow lane are clearly traced by the streak lines on each side. Unsteady flow activities are minimal behind rows 1–4, and so oscillatory motion is hardly discernible on the video screen at these portions of the flow lane. The flow becomes gradually more active as it moves deeper inside the bundle. In fact, some rotational motion of the flow is apparent in the shear layers on both sides of the flow lane behind the fifth row. These activities develop into well-defined vortices behind rows 7 and 8, as observed in Figure 10. The periodic nature of the flow pattern is illustrated by the hot-film spectra measured behind rows 1 and 5 that are given in Figure 10. Both spectra contain clear peaks, although little unsteady activity is visually evident behind these rows. The peaks have the same frequency, but the amplitude of the peak measured behind row 1 is an order of magnitude smaller than that measured behind row 5. These features, in addition to the visualization, illustrate the developing nature of flow periodicity from the front to the rear rows at low Reynolds number.

In Figure 11, the flow patterns visualized for a Reynolds number range of $900 < R < 4530$ are shown. As the Reynolds number is increased, the location at which flow unsteadiness starts to become visible continues to move upstream, as can be followed from the photograph series (a)–(d). The well-defined vortices observed behind rows 8–12 for the lowest Reynolds number case, Figure 10, form already behind the fourth row at $R = 1630$. However, they seem to be less organized than they are at low Reynolds numbers. In fact, they disappear at rows further downstream, and the flow becomes turbulent. This feature is illustrated in the hot-film spectra measured behind the first and fifth rows for R $= 1630$ and are given in Figures 11(e, f). The spectrum measured behind row 1 at $R = 1630$ displays a periodic activity with a frequency corresponding to $S = 1{\cdot}72$. This Strouhal number agrees with the component f_{v3} which is measured in the air tests. The bottom spectrum displays the frequency content of the flow unsteadiness behind the first row at a Reynolds number of 4530. This spectrum does not become totally turbulent and contains a hump indicating the remnant of the component f_{v3}. The Strouhal number calculated with the frequency corresponding to the middle of the hump is found to be 1·72. This value is similar to the Strouhal number of the component f_{v3} measured in air.

3.3. Large Pitch Ratio Array ($X_P = 3{\cdot}41$)

Figure 12 shows three spectra of the fluctuation pressure measured on a tube in the first row of the array with $X_P = 3{\cdot}41$. The Reynolds numbers corresponding to these spectra are 15 000, 30 000 and 43 700, respectively. Each of these spectra displays only one flow periodicity peak corresponding to a Strouhal number of $S = 0{\cdot}22$. In Figure 13, the pressure spectra measured at rows 1–10 at a Reynolds number of $R = 40\,100$ are displayed. The frequency component corresponding to $S = 0{\cdot}22$ seems to be the only periodic component existing in the array regardless of the measurement location. It persists and preserves its narrow-banded character deep inside the array, despite a significant increase in the turbulence level.

The results of the arrays with intermediate and small pitch ratios have shown that the high-frequency components often appear at relatively low Reynolds numbers and subside

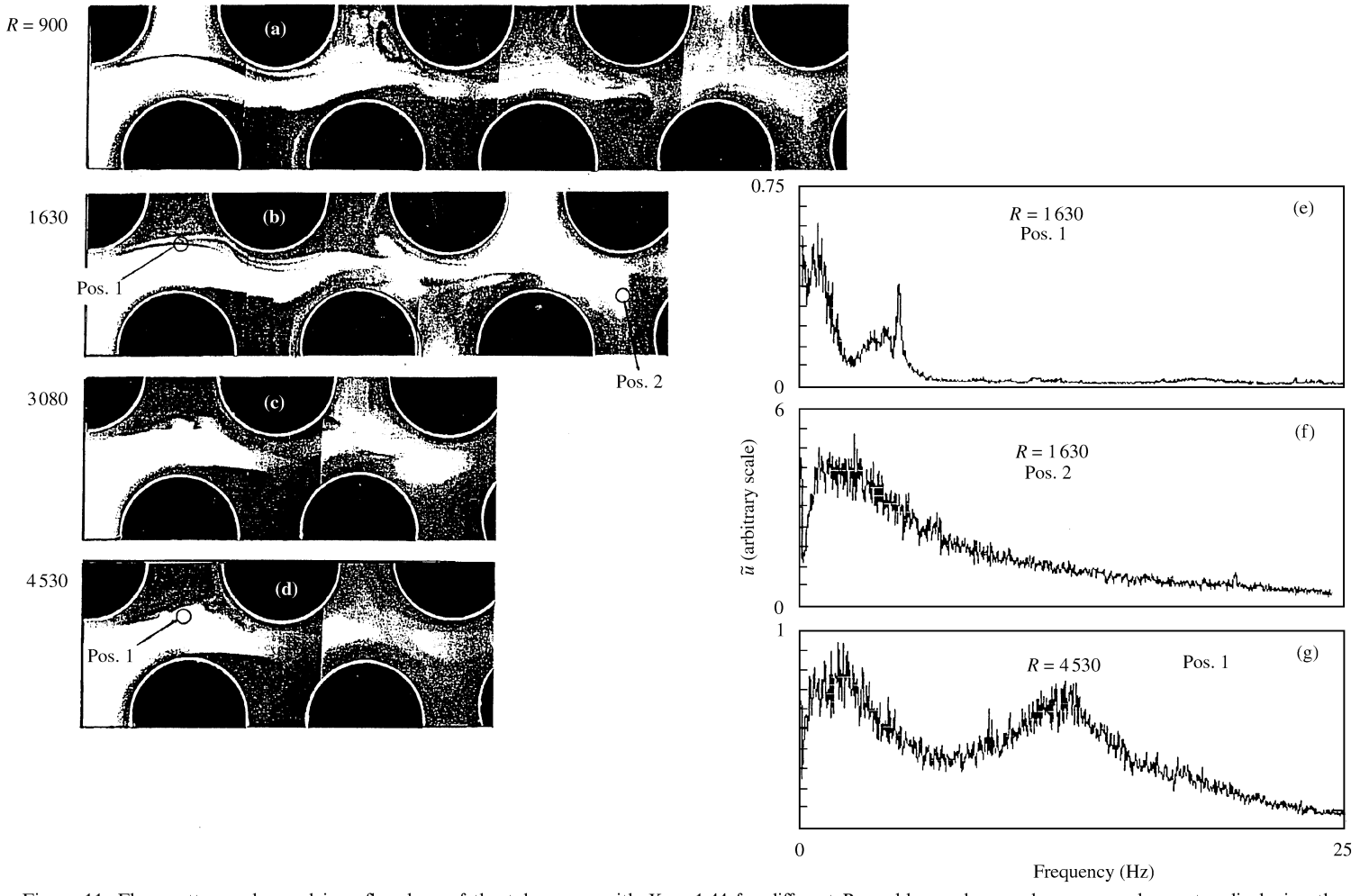

Figure 11. Flow patterns observed in a flow lane of the tube array with $X_p = 1{\cdot}44$ for different Reynolds numbers and some sample spectra displaying the characteristics of the flow oscillations behind rows 1 and 5.

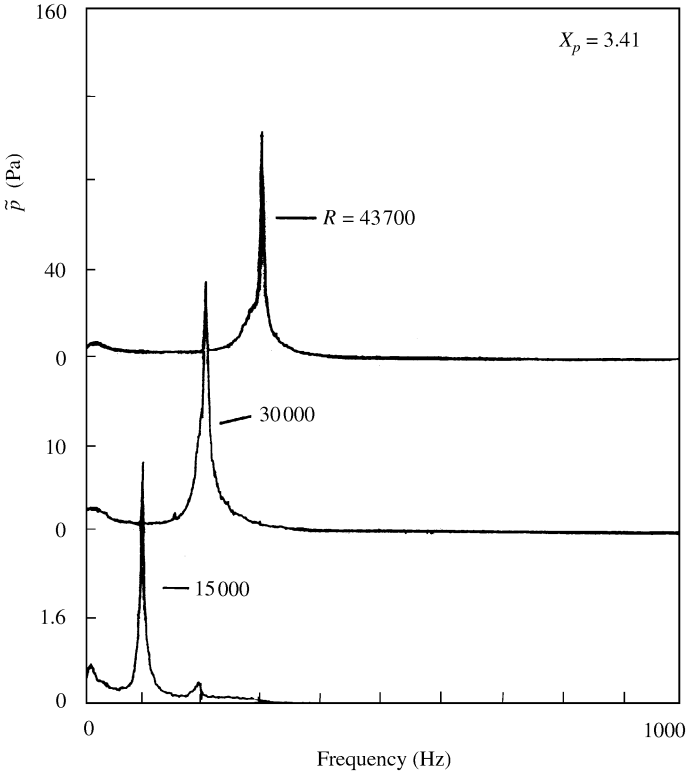

Figure 12. Pressure spectra showing the flow periodicity S_1 at the first row of the large pitch-ratio array ($X_p = 3{\cdot}41$) for three values of Reynolds number.

when the Reynolds number is increased over ~ 6000. The lowest Reynolds number attainable in the air tests of the large pitch-ratio arrays was $R = 5400$. Therefore, in order to find out whether the high-frequency component also exists in large pitch-ratio arrays at low Reynolds numbers, some tests of the same array were carried out in the water channel. The Reynolds number range of these tests was $0 < R < 6500$. The frequency components of the flow periodicities measured by a hot film behind rows 1 and 5 of this array are plotted against the gap velocity in Figure 14. Two flow periodicity components are detected in this Reynolds number range, $S_1 = 0{\cdot}22$ and $S_2 = 0{\cdot}31$. The component S_1 corresponds exactly to that measured in air. As observed in Figure 14, the high-frequency components occur mainly behind the front rows and at low Reynolds number ($R < 2750$), whereas the low-frequency component exists behind the inner rows at all Reynolds numbers. The high-frequency component disappears altogether when the Reynolds number is increased over 2750 and thereafter the low-frequency component dominates the whole array.

Figure 15 shows four sets of flow vizualisation photographs illustrating the flow patterns occurring behind rows 1–7 of this array in the Reynolds number range of $340 < R < 5660$. As expected, well-defined vortices are shed ($S = 0{\cdot}32$ from video counting) from these tubes in the case with the lowest R [Figure 15(a)]. The vortices shedding from the tubes of each tube column seem to form a wake developing along this column; however, a special phase relation between the wakes of different tube columns could not be determined. When the Reynolds number is increased to 830 [Figure 15(b)], the same pattern

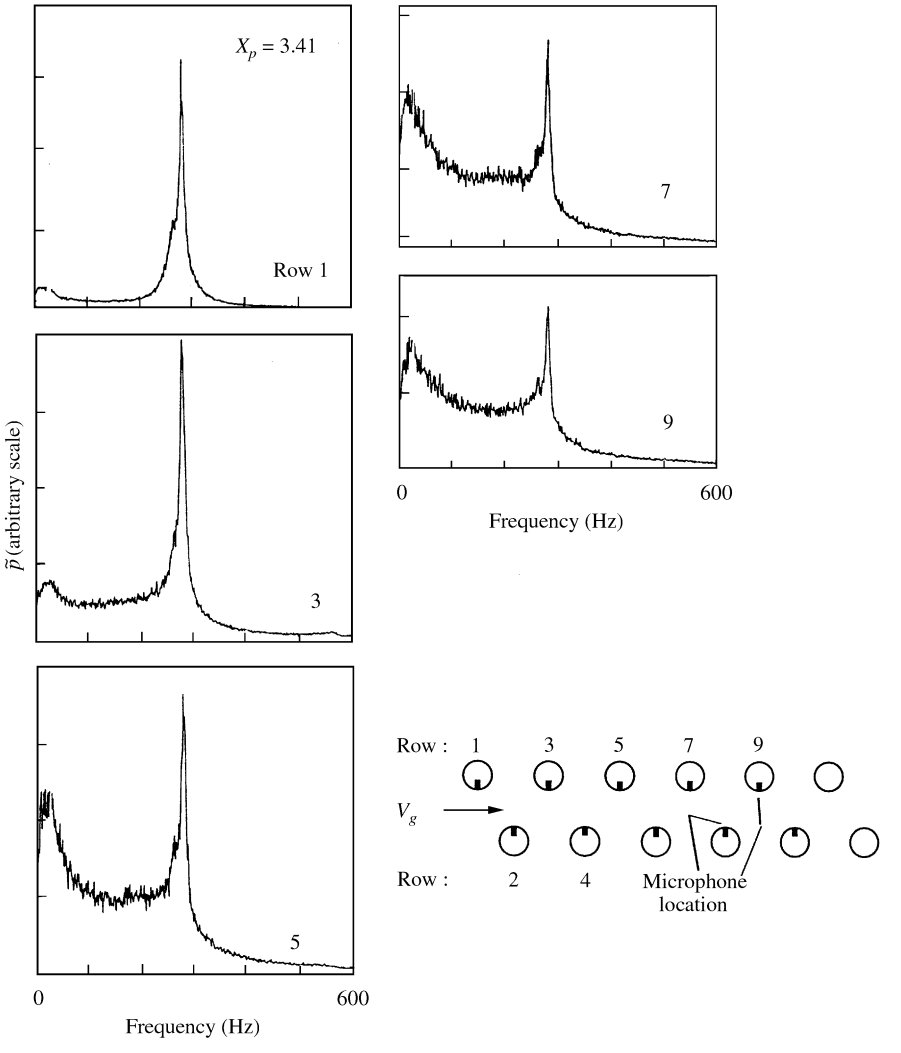

Figure 13. Pressure spectra showing the flow periodicity S_1 at five different rows (from row 1 to 9) in the large pitch-ratio array ($X_p = 3{\cdot}41$) for a Reynolds number of R = 40 100.

persists except in the wakes of the second row. The vortices forming in these wakes become prone to the instability of the shear layers separating from the tubes of this row, resulting in a substantial increase in the formation length and a decrease in the vortex size. In fact, the flow structure behind the second row depicts a shear-layer oscillation pattern rather than alternating wake shedding. Similar changes are also observed to occur behind the first row tubes when the Reynolds number is further increased to $R = 1800$ [Figure 15(c)].

A significantly different flow pattern occurs in the high Reynolds number case, Figure 15(d). In this case, instead of a wake structure developing along the tube columns, an independent wake structure composed of two vortices forms behind each tube of the array. A Strouhal number of 0·22 was calculated from the frequencies of these vortices by means of video counting. This value agrees with the frequency component f_{v1} measured in the air tests of this array.

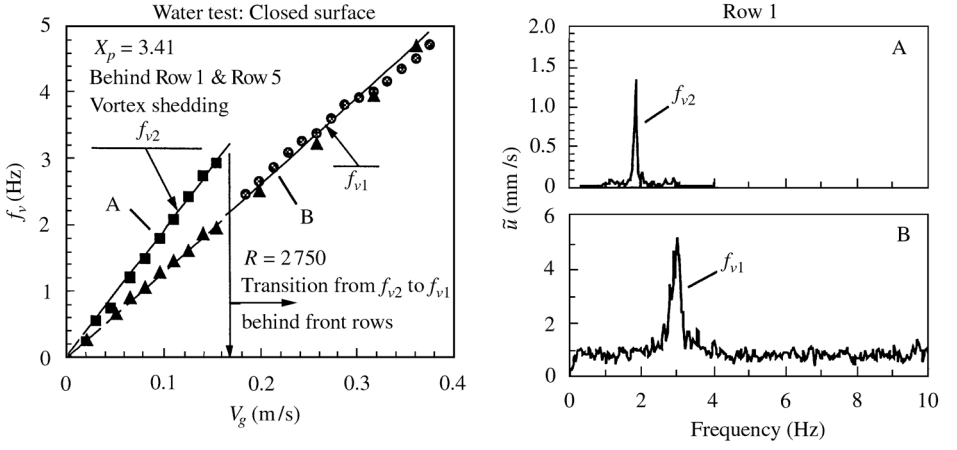

Figure 14. Frequency components of the flow periodicities observed behind rows 1 and 5 in a large pitch-ratio array with $X_p = 3{\cdot}41$ as a function of gap velocity, and two hot-film spectra measured behind row 1 at velocities corresponding to points A and B. ■, ●, behind row 1; ▲, behind row 5.

4. STROUHAL NUMBER OF VORTICITY SHEDDING

The Strouhal numbers of the flow periodicities of all the tested arrays are given in Figure 16 as a function of tube pitch ratio. The data collected from the literature are also included in this chart for comparison purposes. Since the data obtained from resonance cases may not always represent those of the natural flow periodicities, they are not included in Figure 16. The Strouhal number in this chart is based on the frequency of flow periodicity, f_v, and the tube diameter, d, and is given by the relation

$$S = f_v d / V_g, \tag{1}$$

where the gap velocity, V_g, is defined as

$$V_g = [(2X_p \cos 30)/(2X_p \cos 30 - 1)]\, V_u. \tag{2}$$

The Strouhal number data are seen to collapse mainly around three different Strouhal number lines in Figure 16. The line S_1 is associated with the lowest frequency observed in the present study and in the studies found in the literature. It corresponds to the frequency component f_{v1}, which dominates at deeper rows but is hardly discernible behind front rows at low Reynolds numbers.

This component has been observed in the pitch-ratio range of $1{\cdot}38 < X_p < 4{\cdot}17$. The only data belonging to S_1 in the range $X_p < 1{\cdot}71$ is reported by Weaver & Grover (1978) for a small pitch-ratio array with $X_p = 1{\cdot}38$. However, it should be mentioned that this data point has been obtained from broad-band turbulence spectra, which do not contain any discrete peaks. The Strouhal number is calculated from the frequency corresponding to the amplitude maxima of these turbulence spectra. This component could not be detected in the present study in the range $X_p < 1{\cdot}71$. S_1 has a value of 0·4 for $X_p = 1{\cdot}38$ and it approaches a value of $\sim 0{\cdot}2$ in arrays with pitch ratios larger than 3, as illustrated in Figure 16.

The Strouhal number line S_2 in Figure 16 corresponds to the frequency component f_{v2}. This component was detected only in the pitch-ratio range $1{\cdot}71 < X_p < 3{\cdot}41$ in the present study. It could be detected only in water tests for $X_p = 2{\cdot}08$ and 3·41, where the Reynolds number is relatively low. Strouhal numbers similar to S_2 have been reported by Chen (1968) and Chen & Weber (1970) for a smaller pitch-ratio array with $X_p = 1{\cdot}25$. However, the

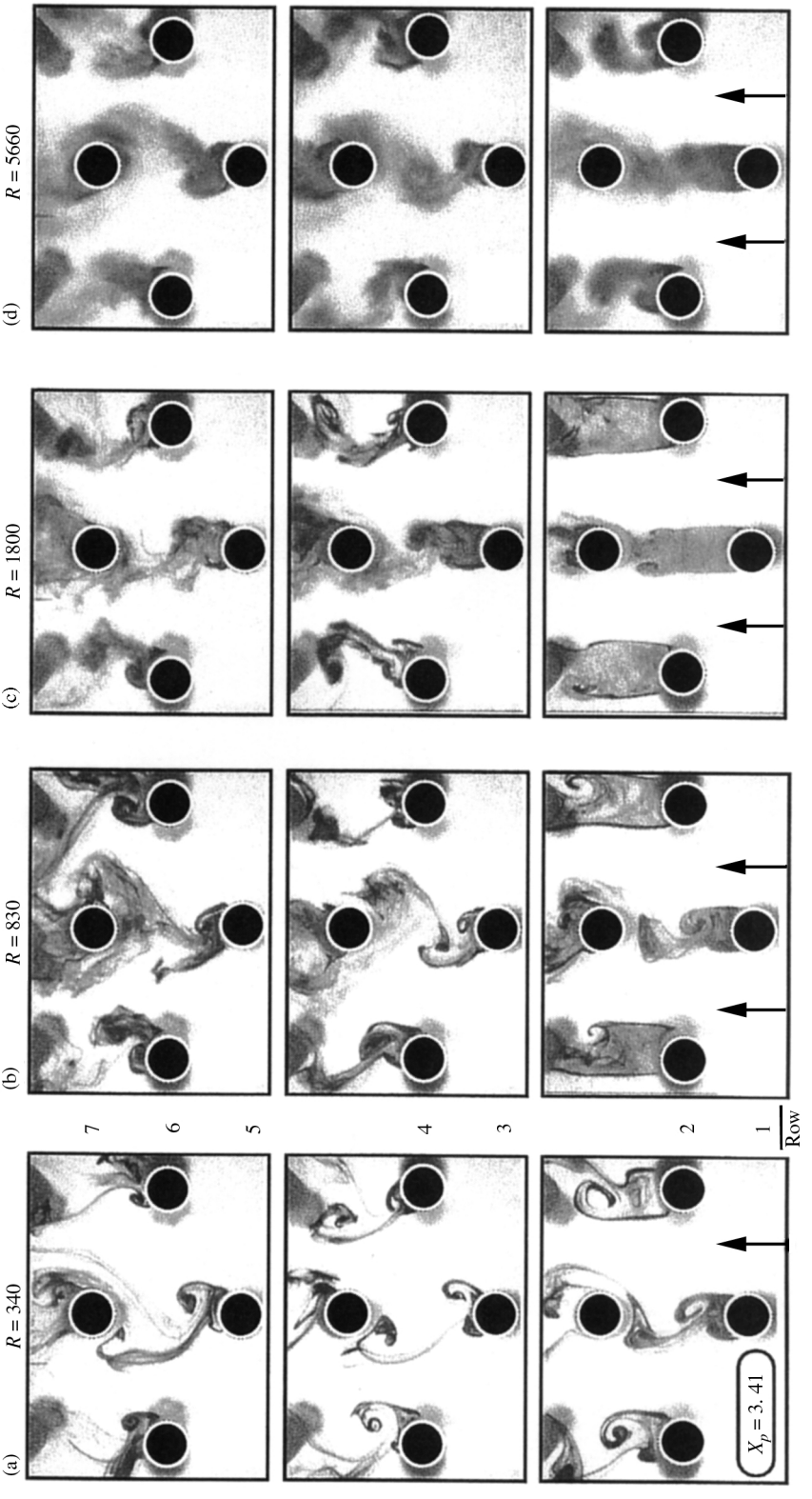

Figure 15. Flow patterns in the large pitch-ratio array ($X_p = 3{\cdot}41$) showing the transition of the flow periodicity from (a) Strouhal number S_2 to (d) Strouhal number S_1 as the Reynolds number is increased from 340 to 5660.

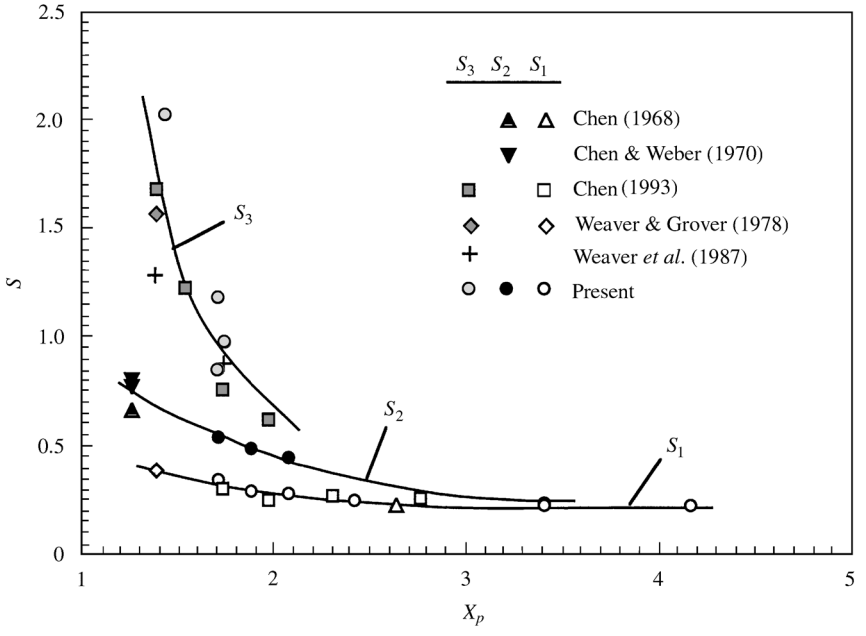

Figure 16. Strouhal number chart for flow periodicities observed under nonresonant flow conditions in parallel triangle arrays, including data from the literature.

existence of S_2 in small pitch ratio arrays could not be verified by the tests of the present study in arrays having $X_p = 1{\cdot}21$ and $1{\cdot}44$. The S_2 component is found to exist simultaneously with the S_1 component and appears to be bound to the front rows only.

The Strouhal number designated with the line S_3 appears to be the characteristic of relatively small pitch-ratio arrays ($X_p < 2$). A wide scatter is observed in the data belonging to this group of Strouhal number. However, the present data agree well with those reported by Chen (1993). In fact, for some geometries, more than one data point seems to appear around the S_3-line. This Strouhal number is associated with the shear-layer vortices developing in the flow lanes between the adjacent tube columns from the first row towards the rear rows, as discussed in Section 3. Therefore, the occurrence of this component is strongly Reynolds number dependent. While it is detected throughout the array at very low Reynolds numbers, it disappears totally at high Reynolds numbers.

5. ACOUSTIC RESPONSE OF PARALLEL TRIANGLE ARRAYS

The acoustic responses of the arrays tested in this study are depicted in Figure 17, which shows the frequency and the sound pressure levels of the acoustic modes as functions of the gap velocity. The main frequency components of the natural flow periodicities are also shown by the solid lines to assess their role in exciting acoustic resonances. The dashed lines in Figure 17 represent the acoustic Strouhal numbers, S_a, which are based on the resonance frequency and the flow velocity at the onset of resonance. In the following, the acoustic response of each array is discussed, with special attention given to the relation between the acoustic Strouhal number(s) and those associated with the natural flow periodicities.

The results of the arrays with $X_p = 1{\cdot}21$ and $1{\cdot}44$ are displayed in Figure 17(a, b). These results are typical of small pitch-ratio PTR arrays. In the case of $X_p = 1{\cdot}21$, despite the presence of a well-defined flow periodicity in the array, the first acoustic mode is *excited not*

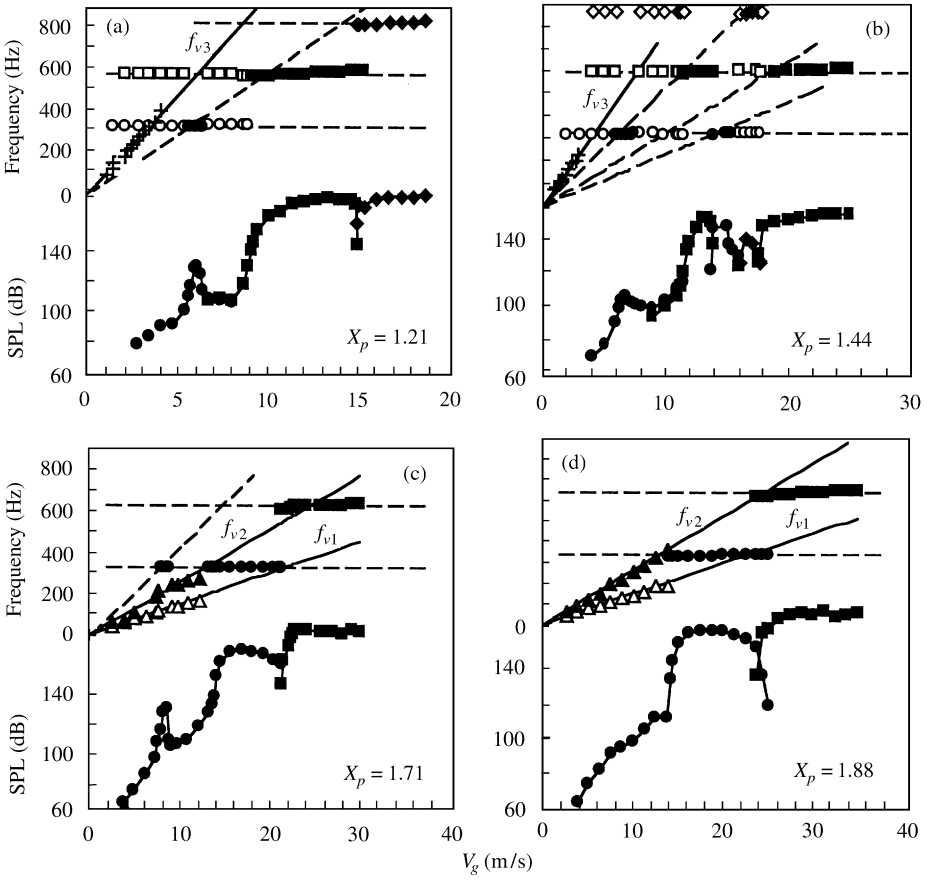

Figure 17. Acoustic responses of the parallel triangle tube arrays tested in this study. The periodic flow components are also shown in each case to help assess their relation to the resonances observed. +, △, ▲, Flow periodicity components; ●, ■, ◆, are the 1st, 2nd and 3rd mode resonances, respectively.

at the point of frequency coincidence but at a substantially higher velocity (about 60% higher than the coincidence velocity). As the flow velocity is increased further, the second and third acoustic modes are also excited. In fact, the resonances of these modes are very strong and have wide ranges of lock-in, although no periodic flow activities exist at these high velocities. The resonances seem to occur according to an acoustic Strouhal number relation (the dashed line) which could not be associated with the natural flow periodicity.

The array with $X_p = 1{\cdot}44$ displays similar characteristics, i.e., the flow periodicity could not be associated with the onset of acoustic resonances in this array. The lowest Strouhal number of flow periodicity was found to be $S = 1{\cdot}72$, whereas the highest S_a of the acoustic resonances was 1·4. In addition, acoustic resonances are observed to occur at two other Strouhal numbers which are even lower than 1·4. These features indicate that acoustic resonances are excited by a flow mechanism other than the natural flow periodicity which dominates before the onset of resonances.

The acoustic responses of the arrays with $X_p = 1{\cdot}71$, 1·88 and 2·08 are illustrated in Figure 17(c–e). These responses exemplify the acoustic behaviour of PTR arrays with intermediate pitch ratios. In the three cases, strong resonances with wide lock-in ranges occur at the first and second acoustic modes. Figure 17 also shows that two dominant

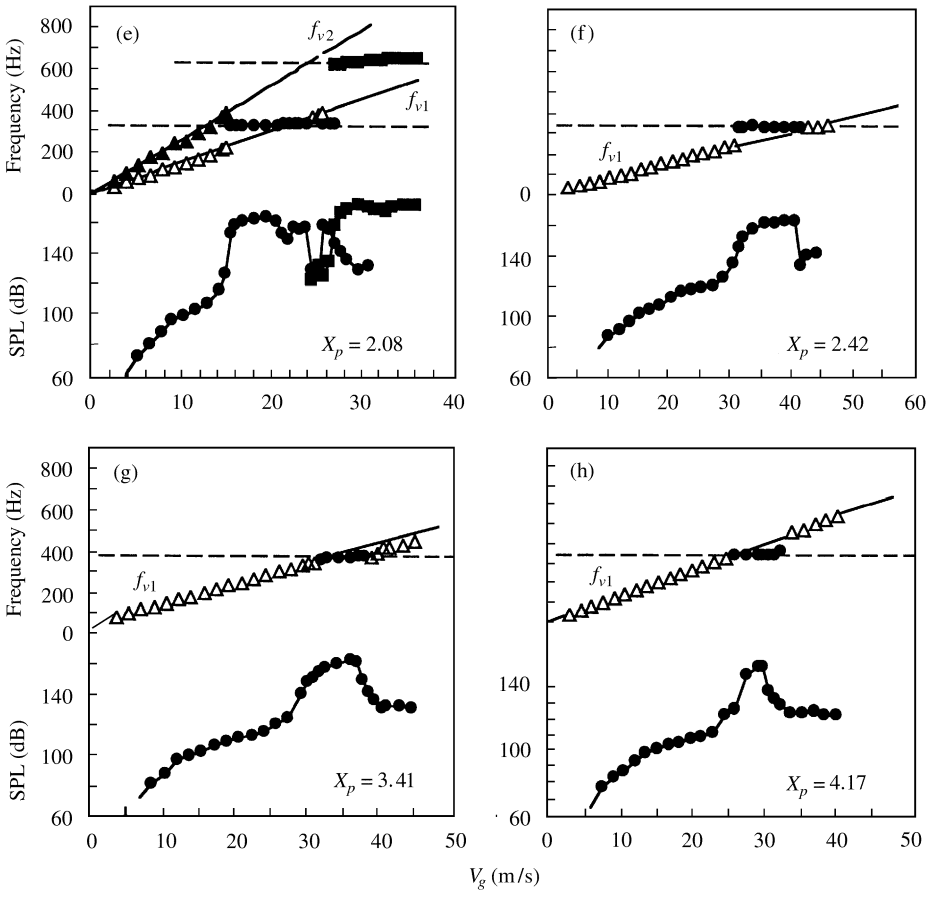

Figure 17. Continued.

components of flow periodicity exist in the three arrays. The high-frequency component is seen to follow a Strouhal number line very close to that initiating the acoustic resonance. However, the first mode resonance is initiated after the frequency of this component is increased beyond the coincidence point, Figure 17(d, e). Moreover, in the array with $X_p = 1{\cdot}71$, a first mode resonance sets-in and subsides at velocities which are much lower than that corresponding to the frequency coincidence. These features suggest that, for intermediate pitch ratios, the flow periodicities present at nonresonant conditions are not directly related to the "acoustic" Strouhal number at the onset of resonances.

Figure 17(f) illustrates the acoustic response of the array with $X_p = 2{\cdot}42$. Only a single periodic flow component exists in this array, corresponding to a Strouhal number of 0·25. The first mode is seen to be strongly excited, reaching a maximum level of more than 160 dB. Acoustic resonance in this array occurs in a manner different from that discussed above. The resonance is initiated at a flow velocity which is substantially lower than that corresponding to the frequency coincidence. Although this feature can be regarded as a lock-in effect, it is remarkable that the resonance subsides when its frequency coincides with that of the natural flow periodicity. In fact, similar behaviour is observed for $X_p = 2{\cdot}08$, Figure 17(e); the first mode resonance subsides at the condition of frequency coincidence between f_{v1} and f_{a1}, and is then recovered as the flow velocity is slightly increased beyond

the coincidence condition. This suggests that the natural vorticity shedding component f_{v1} and the resonant acoustic field cannot coexist in this particular case, i.e., for $2{\cdot}08 \leq X_p \leq 2{\cdot}42$. This acoustic behaviour is similar to that observed for some in-line tube arrays (Oengören & Ziada 1992a).

The acoustic responses of two arrays with large pitch ratios ($X_p = 3{\cdot}41$ and $4{\cdot}17$) are presented in Figure 17(g, h). In contrast to the cases discussed so far, the acoustic resonance in these arrays occurs in a classical manner such that it is initiated when the frequency of flow periodicity approaches the frequency of the first acoustic mode. A lock-in range is observed after which the flow periodicity is recovered at its original natural Strouhal number ($S = 0{\cdot}23$). For these large pitch-ratio arrays, classical vortex shedding in the tube wakes generates the vorticity-shedding excitation. This excitation is known to be capable of coupling with the transverse acoustic modes of the test section and thereby generate strong acoustic resonances.

6. ACOUSTIC STROUHAL NUMBERS

The acoustic responses of the arrays investigated in this study have indicated that for most of these arrays, the critical velocities at which acoustic resonances set in cannot be predicted from the Strouhal numbers of the natural flow periodicities, which are detected at nonresonant conditions. As discussed in the preceding section, for parallel triangle arrays with $X_p < 2{\cdot}42$, acoustic resonances set in at velocities significantly different from those at which the frequency of the natural flow periodicity coincides with the acoustic resonance frequency. This feature of parallel triangle arrays is different from that of normal triangle arrays, for which the acoustic Strouhal numbers have been found to approximate those of the natural flow periodicities (Oengören & Ziada 1998).

As mentioned earlier, the observed acoustic behaviour of parallel triangle arrays is found to be similar to that of in-line arrays, which has been investigated in some detail by Ziada *et al.* (1989) and Oengören & Ziada (1992a). This similarity seems to stem from the fact that both array patterns allow the flow to proceed freely along the flow lanes between the tube columns. Thus, as in the case of in-line arrays, vorticity shedding in PTR arrays seems to be generated by the instability of the jets which develop along the flow lanes. Acoustic resonances, however, are excited by either alternating vortex shedding or by shear-layer instability, and therefore the Strouhal number at the onset of resonance may deviate substantially from that of the natural vorticity shedding.

In order to be able to predict the onset of acoustic resonance in parallel triangle arrays, an acoustic Strouhal number chart has been developed and is given in Figure 18. The acoustic Strouhal number, S_a, is defined as

$$S_a = f_a d / V_{gr}. \tag{3}$$

where f_a is the acoustic resonance frequency and V_{gr} is the critical gap velocity at the onset of acoustic resonance.

As observed in Figure 18, multiple acoustic Strouhal numbers exist in arrays with $X_p < 1{\cdot}71$. Although some of these Strouhal numbers are associated with the resonance of all modes (from 1 to 3), some are related to only one mode. To avoid any misunderstanding, the acoustic modes excited by each Strouhal number are noted near each data point in Figure 18. The curve displayed in this figure is the upper limit to the acoustic Strouhal numbers of the tested cases and should be treated as a design value to avoid acoustic resonances over the whole velocity range.

The usage of the acoustic Strouhal number chart for design purposes can be demonstrated by considering the case with $X_p = 1{\cdot}44$, which is illustrated in Figure 17(b). As the

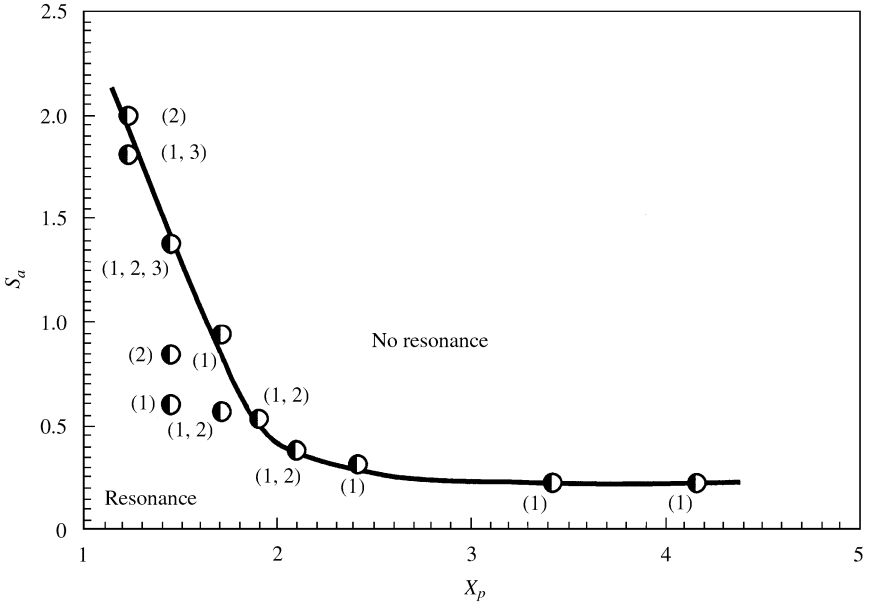

Figure 18. Acoustic Strouhal number chart for parallel triangle arrays developed from the measurements of the present study.

flow velocity was increased, the lowest three acoustic modes were excited in a rather complex order. After the resonance of modes 1 and 2, mode 1 was excited again. This was followed by mode-3 resonance, and finally mode 2. The acoustic Strouhal numbers of these resonances are indicated in Figure 18. From a practical point view, estimation of the critical flow velocities corresponding to these Strouhal numbers is of little use. Instead, the designer should ensure that the Strouhal number based on the maximum flow velocity and any acoustic frequency is higher than the design limit given by Figure 18.

The upper bound of the acoustic Strouhal numbers given in Figure 18 may appear similar to the envelope of the Strouhal numbers of the natural flow periodicities which are depicted in Figure 16. However, this is true only for large pitch ratios, $X_p > 2{\cdot}3$, which is to be expected, since alternating vortex shedding becomes dominant at large pitch ratios. For smaller pitch ratios, S_3 can be up to 54% higher than the acoustic Strouhal number.

Finally, reference should be made to several design criteria which can be used to predict whether an acoustic resonance will actually occur or not, given that the critical flow velocity is within the operating range of the plant. The most recent criterion was originally formulated by Blevins & Bressler (1993) and further developed by Eisinger *et al.* (1996). Comparison with these criteria however is outside the scope of the present study which focuses on the flow phenomena generating periodic flow excitation and acoustic resonance.

CONCLUSIONS

The nature of the flow periodicities and the mechanism of acoustic resonance in parallel triangle tube arrays were investigated by means of wind tunnel experiments. The tests covered a pitch ratio range of 1·21–4·17. In addition, three arrays with small, intermediate and large pitch ratios, $X_p = 1{\cdot}44$, 2·08 and 3·41, were tested in water to visualize the flow mechanisms generating the flow periodicities. The effect of Reynolds number on the spatial

development of the flow mechanisms was investigated and discussed. In all tested cases, resonance conditions for at least the first acoustic mode were reached in the wind tunnel experiments. Thus, the test results provide new insights into the acoustic response of parallel triangle arrays.

Natural flow periodicities in parallel triangle arrays occur at three different Strouhal numbers, S_1, S_2 and S_3. The highest Strouhal number, S_3, is associated with the instability of the shear layer which develops on the sides of the flow lanes between the tube columns. This type of flow periodicity exists only in arrays with pitch ratios smaller than 2. Moreover, they are sustained only at relatively low Reynolds numbers. The Strouhal number S_2 is associated with alternating vortex shedding behind the first two rows. It subsides when the Reynolds number is sufficiently increased and is replaced by the periodicity S_1. The Strouhal number S_1 is associated with alternating, large-scale vortex shedding in the wakes of the inner tubes. It is observed in arrays with $X_p > 1{\cdot}4$ in this study and in the literature. At high Reynolds numbers, this periodicity dominates in the whole array, i.e., also at the front rows. A Strouhal number chart has been developed for the natural flow periodicities in parallel triangle arrays utilizing the data of the present study and the data available in the literature.

For the arrays with $X_p \leq 2{\cdot}42$, the onset of acoustic resonances could not be related to the natural flow periodicities which are observed before the onset of resonances. This contrasts with the acoustic response of normal triangle arrays for which the resonance has been found to be excited by the natural flow periodicities. A chart for the acoustic Strouhal number for parallel triangle arrays has been developed.

The excitation mechanism of acoustic resonance in parallel triangle arrays seems to be similar to that of in-line arrays. The reasons for this similarity must lie in the fact that both arrays allow the flow to proceed along the free-flow lanes between the tube columns, which results in a similar interaction mechanism between the flow instability and the sound waves.

ACKNOWLEDGEMENT

This work was carried out at Sulzer Innotec Ltd before the lead author left to join McMaster University. The authors gratefully acknowledge the financial support by the Swiss National Energy Research Funds, ABB Enertech Ltd and Sulzer Innotec Ltd.

References

Blevins, R. D. & Bressler, M. M. 1993 Experiments on acoustic resonance in heat exchanger tube bundles. *Journal of Sound and Vibration* **164,** 503–533

Chen, Y. 1993 Strouhal periodicity in parallel triangular tube arrays. Masters thesis, McMaster University, Mechanical Engineering, Hamilton, Ontario, Canada.

Chen, Y. N. 1968 Flow-induced vibration and noise in tube bank heat exchangers due to von Karman streets. *ASME Journal of Engineering for Industry* **90,** 134–146.

Chen, Y. N. & Weber, M . 1970 Flow-induced vibrations in tube bundle heat exchangers with cross and parallel flow. *Proceedings of ASME Symposium on Flow-Induced Vibrations in Heat Exchangers*, pp. 57–58. New York: ASME.

Eisinger, F. L., Frances, J. T. & Sullivan, R. E. 1996 Prediction of acoustic vibration in steam generator and heat exchanger tube banks. *ASME Journal of Pressure Vessel Technology* **118,** 221–236.

Oengören, A. & Ziada, S. 1992a Vorticity shedding and acoustic resonance in an in-line tube bundle. Part II: Acoustic resonance. *Journal of Fluids and Structures* **6,** 293–309.

Oengören, A. & Ziada, S. 1992b Unsteady fluid forces acting on a square tube bundle in air cross flow. *Proceedings of ASME/JSME/CSME/IMechE/IAHR International Symposium on Flow Induced Vibrations and Noise, Vol. 1: FSI/FIV in Cylinder Arrays in Cross-Flow* (eds M. P. Païdoussis, W. J. Bryan, J. R. Stenner & D. A. Steininger), pp. 55–74, New York: ASME.

OENGÖREN, A. & ZIADA, S. 1998 An in-depth study of vortex shedding, acoustic resonance and turbulent forces in normal triangle tube arrays. *Journal of Fluids and Structures* **12,** 717–758.
PAÏDOUSSIS, M. P. 1982 A review of flow-induced vibrations in reactors and reactor components. *Nuclear Engineering and Design* **74,** 31–60.
PRICE, J. S., PAÏDOUSSIS, M. P. & MARK, B. 1995 Flow visualisation of the interstitial cross-flow through parallel triangular and rotated square arrays of cylinders. *Journal of Sound and Vibration* **181,** 85–98.
POLAK, D. R. & WEAVER, D. S. 1995 Vortex shedding in normal triangular tube arrays. *Journal of Fluids and Structures* **9,** 1–17.
WEAVER, D. S. 1993 Vortex shedding and acoustic resonance in heat exchanger tube arrays. *Technology for the '90s* (eds M. K. Au-Yang, T. V. Narayanan, K. H. Hsu, S. S. Chen, T. H. Liu & A. G. Ware), pp. 777–810, New York: ASME.
WEAVER, D. S., FITZPATRICK, J. A. & ELKASHLAN, M. 1987 Strouhal numbers for heat exchanger tubes in cross flow. *ASME Journal of Pressure Vessel Technology* **109,** 219–223.
WEAVER, D. S. & GROVER, L. K. 1978 Cross-flow induced vibrations in a tube bank — Turbulent buffeting and fluid-elastic instability. *Journal of Sound and Vibration* **59,** 277–294.
WEAVER, D. S., LIAN, H. Y. &HUANG, X. Y. 1993 Vortex shedding in rotated square tube arrays. *Journal of Fluids and Structures* **7,** 107–121.
ZIADA, S. & OENGÖREN, A. 1992 Vorticity shedding and acoustic resonance in an in-line tube bundle, Part I: Vorticity shedding. *Journal of Fluids and Structures* **6,** 271–292.
ZIADA, S. & OENGÖREN, A. 1993 Vorticity shedding in an in-line tube bundle with large tube spacings. *Journal of Fluids and Structures* **7,** 661–687.
ZIADA, S., OENGÖREN, A. & BÜHLMANN, E. T. 1989 On acoustical resonance in tube arrays. Part 1: Experiments. *Journal of Fluids and Structures* **3,** 293–314.

APPENDIX: NOMENCLATURE

P tube pitch
R Reynolds number based on gap velocity, $R = V_g d/v$
S Strouhal number of vorticity shedding, $S = f_v d/V_g$
S_a Strouhal number of acoustic resonance, $S_a = f_a d/V_g$
V_g gap velocity, $V_g = [(2X_p \cos 30)/(2X_p \cos 30 - 1)]\, V_u$
V_u upstream velocity
V_{gr} critical gap velocity at the onset of acoustic resonance
X_p tube pitch ratio, P/d
d tube diameter
f_v frequency of vorticity shedding
f_a acoustic resonance frequency
$\tilde{p}$ r.m.s. amplitude of pressure fluctuation
$\tilde{u}$ r.m.s. amplitude of velocity fluctuation
v kinematic viscosity